

A Self Adaptive Global Digital Image Correlation Algorithm

L. Wittevrongel · P. Lava · S.V. Lomov · D. Debruyne

Received: 30 April 2014 / Accepted: 21 August 2014 / Published online: 4 October 2014
© Society for Experimental Mechanics 2014

Abstract A novel Digital Image Correlation algorithm is presented, focussing on accurately determining small strains with high strain gradients. Principles from p-adaptive finite element analysis are implemented to obtain a self adapting higher order mesh. The self adapting principle reduces the dependency of the results on the user's input and the higher orders insure sufficient degrees of freedom. Performance of the algorithm, in terms of resolution and spatial resolution, is checked and compared to the traditional local method. The results indicate that the introduced method is appropriate for accurately measuring high heterogeneous deformations and that the obtained data is to a large extent user independent.

Keywords Global · Digital image correlation · Hierarchical · Adaptivity

Introduction

Full field measurement techniques are important techniques used in experimental mechanics as it makes the connection between simulations and experiments. The measured deformation field is used for several purposes such as model validation or material identification [1]. The full-field displacement can be measured using different optical

approaches like speckle interferometry, moiré, holographic interferometry, Digital Image Correlation (DIC), etc [2]. Of these, DIC is a very popular one thanks to its versatility. DIC is a measurement technique which makes it possible to measure displacements at the surface of an object by comparing two white light images. The use of “normal” images and thus standard cameras, explain the growing popularity of DIC as it is easy both to use and set-up. Further advantages of this technique are that measurements are contact-less, strains on the entire surface are determined (so-called “full-field”) and the method is applicable to a wide range of materials and loading conditions. This technique has a traditional, subset-based [3] (local) approach that is very well developed and is widely used in both commercial as well as academic packages. Nevertheless this traditional approach has some important drawbacks, making it cumbersome to be used in some specific applications. One of these applications is strain measurement on experiments producing very small strains with high strain gradients [4]. An alternative method, namely “global approach”, is available in DIC where a complete element mesh is tracked on the images. This method insures C^0 -continuity, resulting in less noise influence. As current global algorithms have a fixed element order and are refined using user experience, measuring these high gradient strains remains cumbersome. In the following, it is proposed to counter these disadvantages by developing a new self adaptive global DIC procedure that uses, when necessary, higher order elements that are able to describe the high gradient displacement field.

This paper is outlined as follows. In section “[Digital Image Correlation](#)”, the main principles of the local and global method are presented. Section “[p-DIC](#)” describes the new method based on the global approach and in section “[Performance](#)” a comparison between local, global and our proposed algorithm is performed. Finally, in section

This publication was supported by Agency for Innovation by Science and Technology in Flanders (IWT).

L. Wittevrongel (✉) · P. Lava · S.V. Lomov · D. Debruyne
Department of Materials Technology, KU Leuven, Campus Ghent, Gebroeders De Smetstraat 1, 9000 Ghent, Belgium
e-mail: lukas.wittevrongel@kuleuven.be



“Application to a Tensile Test”, the local and the adaptive global algorithm are used to correlate a standard tensile test.

Digital Image Correlation

In DIC, the displacement field is found by comparing two images which represent the deformed and undeformed object. Comparing the gray level distribution of these images, and thus determining the displacement field, can be done with two different approaches: using the traditional local approach or the more recently developed global approach. In what follows, both methods will be briefly described.

Local DIC

The local method, also known as the subset method, is the most popular approach for DIC. It is based on tracking each pixel from the reference image to the deformed image [3] and is used in almost all commercial and academic correlation software [5–9]. To track a pixel between images, a certain amount of information is required as the gray value of a pixel by itself is not unique between two images. The information for locating the pixel is found in the so-called subsets, a group of pixels surrounding the considered pixel. The traditional local method uses these subsets in the algorithm, hence the name: “subset method”. The actual tracking of the pixel from the reference to the deformed image is based on optimising a specific correlation function representing the difference of the subset between reference and deformed image. If the subset is located in the deformed image, the displacement of the center of the subset is determined as the displacement for that pixel (see Fig. 1).

An important drawback of this technique is the non-continuity of the displacement field, as the displacement of the pixels are sought separately and thus no interconnectivity is taken into account. This independent approach influences the calculation of the strains, as smoothing in

the noisy displacement field is essential to obtain acceptable strain results [10–12]. For the strain calculation mostly a local polynomial smoothing is used, where a rectangular area denoted as strain window is used. The extend of smoothing is controlled by the subset size, step size and strain window size. Therefore, the measurement result is significantly influenced by these user-dependent parameters [13]. Choosing the subset and strain window relatively large will respectively lead to a good (low) displacement and strain resolution because a lot of data is used to track the pixel. By using these larger values averaging will occur, leading to a higher spatial resolution which is less desirable. Consequentially, opting for smaller values will automatically lead to reducing spatial resolution but increasing displacement/strain resolution [14]. Definitions of these resolutions are found in section “Methodology”. Other disadvantages are that data is only known at the centres of calculated subsets, separated by the step, leading to a sparse set of data points and the lack of information around the edges, as a distance of half a subset of the pixel towards the edge need to be preserved. Increasing density of data is possible by decreasing the step size (e.g. 1) but this results in significantly longer calculation time.

Global DIC

The second approach for DIC is the global DIC method. Compared to the subset method, where pixels are individually tracked, the global method tracks all pixels within the test object simultaneously. Thus instead of tracking subsets, a complete mesh is tracked. This method was initially proposed by Cheng et al. [15]. Later, Besnard et al. developed the Q4-DIC [16], where a fixed bilinear (Q4) or quadratic (Q8) mesh is implemented. In the following the principle of global DIC is presented. The images used in the correlation, representing the original and deformed surface of the tested specimen, can be represented by 2D functions $f(\mathbf{x})$ and $g(\mathbf{x})$, defining (interpolated) gray values at position $\mathbf{x} = (x, y)$. Using the conservation of optical flow, the problem can be described as determining \mathbf{d} , the unknown displacement field for an element Ω_e , so that for each point \mathbf{x} element of Ω_e :

$$f(\mathbf{x} - \mathbf{d}) = g(\mathbf{x}). \quad (1)$$

This is valid if no external influences such as light conditions, noise and other external parameters are considered. Because these influences do act upon the images, specific cost functions are used to minimize the difference between $f(\mathbf{x} - \mathbf{d})$ and $g(\mathbf{x})$. The correlation functions that will be used in the implementation are NSSD (Normalised Sum of Squared Differences) and ZNSSD (Zero Normalised Sum of Squared Differences) (equivalent to NCC and ZNCC [17]), used to cope with offset and scaling in light conditions

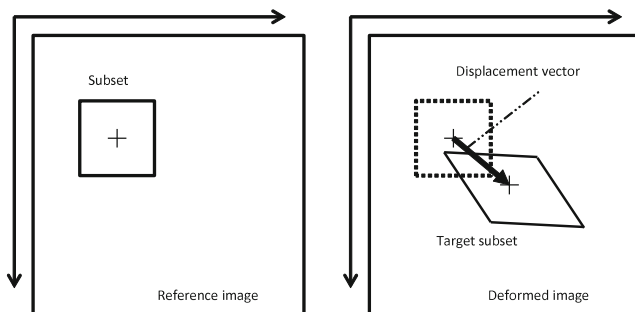


Fig. 1 Principle of the subset-based DIC, tracking of a pixel from reference to deformed image

[18]. Here, to maintain simplicity, the SSD (Sum of Squared Differences) is used to present the method:

$$\epsilon^2 = \iint_{\Omega_e} ([f(\mathbf{x} - \mathbf{d}) - g(\mathbf{x})]^2) d\mathbf{x} \quad (2)$$

When substituting the first order Taylor expansion of $f(\mathbf{x} - \mathbf{d})$ into equation (2) the cost function becomes:

$$\epsilon^2 = \iint_{\Omega_e} ([-\mathbf{d} \cdot \nabla f(\mathbf{x}) + f(\mathbf{x}) - g(\mathbf{x})]^2) d\mathbf{x} \quad (3)$$

Introducing a pre-described function for \mathbf{d} [19], the displacement within element Ω_e object of the mesh Δ , on an arbitrary basis Φ_i as

$$\mathbf{d} = \sum_{i,a} \Phi_i \delta_{ia} \mathbf{e}_a \quad (4)$$

Where i is the number of shape functions used, a are the system directions and δ_{ia} are the displacement parameters. Minimising equation (3) with respect to δ_{ia} , yield a linear equation:

$$[K_{ijab}]^e [\delta_{ia}]^e = [F_{jb}]^e \quad (5)$$

with:

$$[K_{ijab}]^e = \iint \Phi_i [\nabla_a f] \Phi_j [\nabla_b f] d\mathbf{x} \quad (6)$$

$$[F_{jb}]^e = \iint [g(\mathbf{x}) - f(\mathbf{x})] \Phi_j [\nabla_b f] d\mathbf{x} \quad (7)$$

Where e is the element number and ∇_a is the derivative of the function to a . Note that $a, b \in \{x, y\}$. Iterative calculation is critical as a Taylor expansion is used, and thus the calculated displacements are an approximation of the real displacement. In the previous algorithm [16] this done by re-correlating a deformed image that is shifted with the integer value of the previously calculated displacement. In the proposed algorithm no image shifting is used as it introduces extra uncertainties. Instead an extra displacement \mathbf{d}' is introduced, representing the previous displacement field. The equation used in this proposed algorithm (in contrast to equation (1)):

$$f(\mathbf{x} - \mathbf{d}) = g(\mathbf{x} + \mathbf{d}'). \quad (8)$$

Resulting in element equations:

$$[K_{ijab}]^e = \iint \Phi_i [\nabla_a f] \Phi_j [\nabla_b f] d\mathbf{x} \quad (9)$$

$$[F_{jb}]^e = \iint [g(\mathbf{x} + \mathbf{d}') - f(\mathbf{x})] \Phi_j [\nabla_b f] d\mathbf{x} \quad (10)$$

This means that now the extra displacement, relative to the previous calculated displacement \mathbf{d}' , can be determined by solving the equation (5) containing a matrix $[K]$ and a matrix $[F]$ which are both based on the gray values of the reference and deformed image. Obtaining \mathbf{d} using δ_{ia} and adding \mathbf{d}' to it results in the complete displacement field.

This displacement field can then be used in the next iteration. It is worth noting that at this stage no interconnectivity between elements is included and that although the equation contains a K and F matrix, similar to stiffness and force matrix in finite element analysis (FEA), no constitutive material laws are used. The solution of the element equation (5) to δ_{ia} , results in \mathbf{d} (described by equation (4)) representing a displacement field within Ω_e .

Solving the system for all the elements of mesh Δ results in a displacement field for each element in the mesh separately without any interconnectivity, and therefore no C^0 -continuity is taken into account. To include this connectivity, all element equations are assembled to one linear “system equation”:

$$[K]^s [\delta] = [F]^s \quad (11)$$

It is common practice to combine the element matrices into the system matrix as it is analogous to FEA [19]. Solving this system will result in a matrix δ containing all separate δ_{ia}^e , but now with the connectivity taken into account.

The global description above was mainly developed by Besnard et al. [16]. A comparison with the local DIC method [20] proved this concept of global DIC. Several algorithms based on the global DIC method have been developed during the years [15, 16, 21–23], all leaving the polynomial degree of the mesh fixed ranging from linear (Q4) elements to higher order elements. The matching algorithm uses a fixed mesh, with the pre-described degree of freedom (DOF) determined by the element order, to determine the displacement field as described above. The element size and pre-described DOF are critical for a good solution as they influence the displacement/strain and spatial resolution the same way a subset does [23]. When extra spatial resolution is needed, refinement of the mesh is done by the user based on his experience. In this context refinement refers reducing the element size. This type of refinement is called h-refinement, where h denotes the element size. In our proposed method principles from the adaptive finite element are adopted in the algorithm to overcome this problem of user based refinement.

The New Approach

The new approach is developed to fulfil the desire of minimising the error due to discretisation [24], caused by meshing and refinement based on the user’s instinct. In the local method this discretisation is caused by the choice of subset, step and strain window. By using an adaptive mesh, locations where the displacement is rather heterogeneous are automatically refined by an algorithm similar to FEA [25]. To our knowledge this is the first development of a fully self-adaptive global image correlation algorithm. The



new method uses principles like p-adaptive mesh, error estimation and hierarchical shape functions ([19] Chapter 8). The use of these principles lead to a very important advantage: extra degrees of freedom can be introduced gradually if the mesh is unable to describe the imposed displacement. This increase of freedom is done automatically, triggered by an error estimator, so the data becomes less user dependent. This method will be referred to as p-DIC and is presented in the following chapter.

p-DIC

General Description

In the derivation of the global approach, following description for the displacement was used:

$$\mathbf{d} = \sum_{i,a} \Phi_i \delta_{ia} \mathbf{e}_a \quad (12)$$

where Φ_i denote the shape functions of the used basis [19]. Such a basis is usually expressed in local coordinates to obtain a more general and generic description. An element described in these local coordinates is a square element where local coordinates $[\xi, \eta]$ are within the range of $[-1..1]$ (so-called master-element, see Fig. 2).

The transformation of the local coordinates $\xi = [\xi, \eta]^T$ into the global coordinate $\mathbf{x} = [x, y]^T$ can be calculated using mapping functions X^e and Y^e :

$$\mathbf{x} = [x, y]^T = [X^e(\xi, \eta), Y^e(\xi, \eta)]^T \quad (13)$$

When a p-adaptive mesh (elements can transform to higher orders) is used, elements are usually larger than the ones

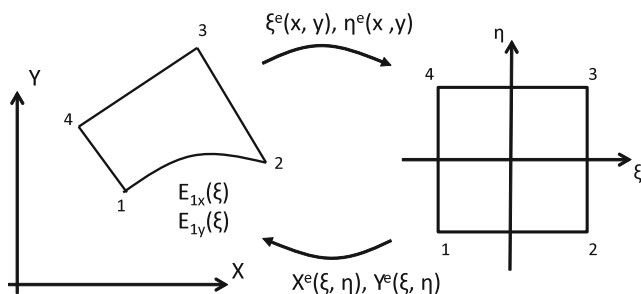


Fig. 2 Mapping coordinates from global to local coordinate system

used in h-refinement. Using these larger elements makes the traditional linear mapping not accurate enough and more precise mapping is necessary. Therefore, in contrast to previous global algorithms, not only the four corner nodes of the element are used for the mapping, but extra functions are blended with the linear functions to obtain a more precise mapping [26]. These functions, denoted by E_j , describe the shape of edge j and are defined as parametric functions $E_j = [E_{jx}(\chi), E_{jy}(\chi)]^T$, where χ is the local coordinate. Using these edge shape functions E_j and the linear node functions $N_i(\xi, \eta)$ defined as:

$$N_i(\eta, \xi) = \frac{1}{4}(1 + \xi_i \xi)(1 + \eta_i \eta) \quad (14)$$

where (ξ_i, η_i) denotes the local coordinates of the i^{th} node, the mapping functions are defined as:

$$\begin{aligned} X^e(\xi, \eta) = & \frac{1}{2}(1 - \eta)E_{1x}(\xi) + \frac{1}{2}(1 + \xi)E_{2x}(\eta) \\ & + \frac{1}{2}(1 + \eta)E_{3x}(\xi) + \frac{1}{2}(1 - \xi)E_{4x}(\eta) \\ & - \sum_{i=1}^4 N_i(\xi, \eta)x_i \end{aligned} \quad (15)$$

$$\begin{aligned} Y^e(\xi, \eta) = & \frac{1}{2}(1 - \eta)E_{1y}(\xi) + \frac{1}{2}(1 + \xi)E_{2y}(\eta) \\ & + \frac{1}{2}(1 + \eta)E_{3y}(\xi) + \frac{1}{2}(1 - \xi)E_{4y}(\eta) \\ & - \sum_{i=1}^4 N_i(\xi, \eta)y_i \end{aligned} \quad (16)$$

where x_i and y_i denote the global coordinate of node i . It is important to notice that no iso-parametric description, where shape and mapping functions are the same, is used but that shape and mapping functions are independent of each other. The choice of shape functions (defining the displacement) is critical as they must be capable of coping with the updating procedure of an adaptive finite element mesh. The shape functions used are hierarchical functions, the same functions as used in p-adaptive finite elements. More specific, the shape functions used are based on Legendre polynomials and are shown in [Appendix](#).

The most important property of these hierarchical basis is that, in contrast to the shape functions used in traditional FEA, higher order shape functions will not influence the shape functions of lower orders. This property of independent hierarchical shape functions lead to the interesting characteristic that refining an element, introducing higher orders, does not influence the already calculated parameters for $[K]$ and $[F]$. This property is illustrated in section “[Adaptivity](#)”.

As mentioned above the shape functions are expressed in local coordinates. It is generally believed that the reversed

mapping functions can not be explicitly determined [27]. Therefore the hierarchical shape functions Φ_i cannot be found in the global $[x, y]$ system analytically and thus the coefficients from equation (9) can not be calculated directly. Consequently a transformation of the element equations from $[x, y]$ to $[\xi, \eta]$ is necessary. The element matrices become:

$$[K_{i_{ajb}}]^e = \iint \Phi_i(\xi, \eta) \nabla_a f(\mathbf{x}(\xi, \eta)) \Phi_j(\xi, \eta) \nabla_b f(\mathbf{x}(\xi, \eta)) \det([J]) d\xi d\eta \quad (17)$$

$$[F_{jb}]^e = \iint (g(\mathbf{x}(\xi, \eta) + d') - f(\mathbf{x}(\xi, \eta))) \Phi_j(\xi, \eta) \nabla_b f(\mathbf{x}(\xi, \eta)) \det([J]) d\xi d\eta \quad (18)$$

Where J is the Jacobian of the system, and $\xi, \eta \in [-1..1]$. Note that $a, b \in \{x, y\}$, and thus still remains in global coordinates.

By transforming the coefficients from a global to a local framework, the element equations are built with local (equals transformed global) shape functions.

$$\Phi_i^l = \Phi_i^g[X^l(\xi, \eta), Y^l(\xi, \eta)] \quad (19)$$

where X^l and Y^l are the mapping functions in element l and Φ_i^l and Φ_i^g are the local and global shape functions. This is based on having the global description for the shape function. In practice, shape functions are given in the local system following the scheme shown in Appendix. In the algorithm the same scheme of assigning shape functions is used. Downside is that choosing local functions instead of transformed global functions obstructs the assembly process of the system equations. This obstruction is explained in following reasoning. When a certain object, node or edge, has more than one element (e.g. common edge between two elements) it has as much local shape functions as it has common elements. The use of transformed global shape functions as local functions insures that all local functions for the same object transform back to the same global shape function, which is necessary for the assembling process.

$$\begin{aligned} \Phi_i^l[\xi^1(x, y), \eta^1(x, y)] &= \Phi_i^g[\xi^2(x, y), \eta^2(x, y)] \\ &= \Phi_i^g[x, y] \end{aligned} \quad (20)$$

where

$$\begin{aligned} \Phi_i^1 &= \Phi_i^g[X^1(\xi, \eta), Y^1(\xi, \eta)] \text{ and} \\ \Phi_i^2 &= \Phi_i^g[X^2(\xi, \eta), Y^2(\xi, \eta)] \end{aligned} \quad (21)$$

Assuming that ξ^1, η^1, X^1, Y^1 and ξ^2, η^2, X^2, Y^2 are the mapping functions of respectively common element 1 and 2 and Φ_i^g is the global shape function. In words, we can describe the condition as: “The equations can be assembled to the system equations if each object copes with the fact that all local shape functions have the same transformed

global shape function”. When locally assigned shape functions are used this condition is not always met. The problem is illustrated in Fig. 3 for a 3th order edge. The figure clearly indicates that both local functions do not describe the same global function, resulting in inverted parameters for the local element functions.

Here δ_1 will denote a positive horizontal displacement, as δ_2 denotes a negative displacement. On the edge, the shape functions become (see Appendix):

$$\Phi_i^1 = 2\eta^1((\eta^1)^2 - 1) \quad (22)$$

$$\Phi_i^2 = 2\eta^2((\eta^2)^2 - 1) \quad (23)$$

The displacement field is then:

$$u = \delta^1 2\eta^1((\eta^1)^2 - 1) = \delta^2 2\eta^2((\eta^2)^2 - 1) \quad (24)$$

and because $\eta^1 = -\eta^2$ (seen in geometry), previous equation yields:

$$\delta^1 = -\delta^2 \quad (25)$$

Here the condition for system assembly is not met, as δ^1 is inverse of δ^2 and thus both functions describe inverse displacement fields. To satisfy the condition, an inversion of one of the element shape functions has to be done. Instead of inverting the shape function directly, a transformation on the final element equations are performed. For the calculation of the element equations the original, local shape functions are used and when the system is assembled, the element matrices get transformed so the assembly becomes possible. This transformation is done by a general procedure based on the so-called ‘direction’ of the edges as it can be shown that the problem only arises on shape functions of edges with an uneven polynomial order and specific direction.

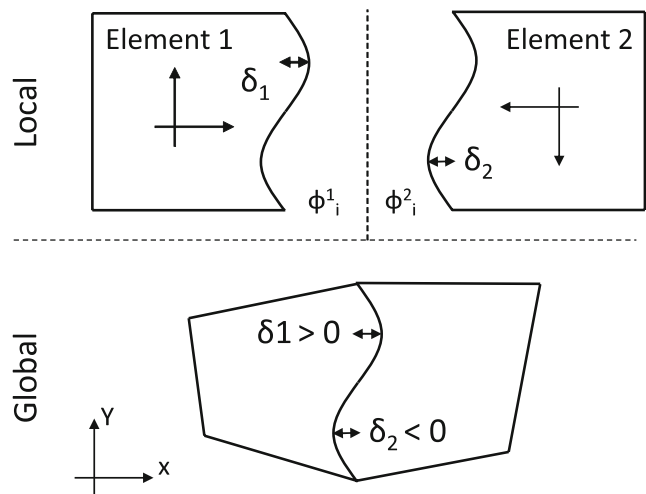


Fig. 3 Visualisation of obstruction in assembly process by the use of locally assigned shape functions



Strain Calculation

As the displacement field is analytical, strains can be derived directly from the displacements. The Green-Lagrange strain tensor is defined as:

$$E = \frac{1}{2}(F^T F - I) = \frac{1}{2}(G + G^T) + \frac{1}{2}G^T G \quad (26)$$

where

$$G = \begin{bmatrix} \frac{\delta d_x}{\delta x} & \frac{\delta d_x}{\delta y} \\ \frac{\delta d_y}{\delta x} & \frac{\delta d_y}{\delta y} \end{bmatrix} \quad (27)$$

Because the displacement field is described in local coordinates, derivatives in matrix G can be calculated using:

$$\begin{Bmatrix} \frac{\delta}{\delta x} \\ \frac{\delta}{\delta y} \end{Bmatrix} = [J]^{-1} \begin{Bmatrix} \frac{\delta}{\delta \eta} \\ \frac{\delta}{\delta \xi} \end{Bmatrix} \quad (28)$$

where

$$J = \begin{bmatrix} \frac{\delta x}{\delta \eta} & \frac{\delta y}{\delta \eta} \\ \frac{\delta x}{\delta \xi} & \frac{\delta y}{\delta \xi} \end{bmatrix} \quad (29)$$

Important is to stress the fact that no smoothing is used to calculate the strains, and accordingly no degradation of spatial resolution in strain is introduced! This is in clear contrast with local DIC methodologies that often use local polynomial smoothing approaches. Previous work indicated that in the subset-based approach nor the derivatives obtained from the Levenberg Marquardt nor the direct derivation from the shape functions can be used to obtain displacement derivatives [13].

Adaptivity

Convergence of the mesh is a key in a good FEA. The same is valid for the global DIC measurement. The displacement and strain field determined by the global (also local) method is the best fit of the mesh, with the allowed degrees of freedom, on the real displacement field. The best fit does not insure that the mesh has enough freedom to sufficiently represent the real deformation field. Correlating a high heterogeneous displacement field with a relative large lower order mesh needs refinement to yield an acceptable solution [19]. Refining the mesh, in this context, means adding extra DOFs to specific edges/faces, so that the mesh is more suitable for representing the actual field. This way of refinement is called p-refinement. In the hierarchical scheme, three basic degrees of freedom can be added (see Appendix and Fig. 4):

- **Nodal or vertex modes:** are the standard DOF for a isoparametric four-noded quadrilateral element. The first order element will only contain these DOFs.
- **Edge or side modes:** are DOF for each edge separately. All edges in an element can contain different DOF.

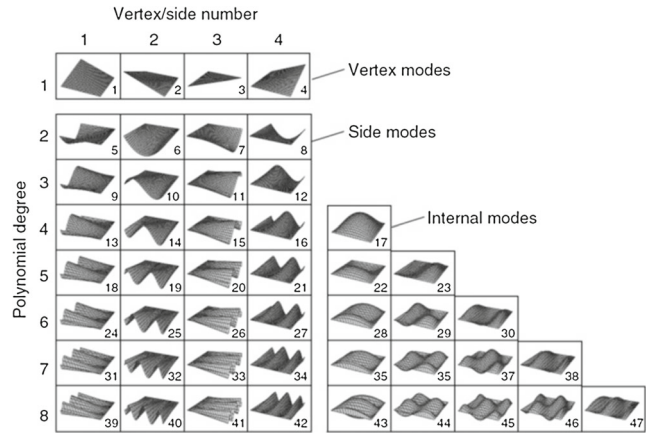


Fig. 4 Visualisation of Legendre shape functions [28]

- **Element or internal modes:** are extra DOFs for one element specific. It only works within an element and does not influence the edges or nodes.

The procedure to refine an element is then straightforward, referring to Fig. 4. Each row represents a specific element order. An element from that order contains all the functions in that row and the ones above. To perform refinement, the element drops a row meaning adding the functions in this new row. Refining from one till three thus means only adding edge modes. Refining to four and higher means adding edge and element modes. This way of updating is possible due to the special nature of hierarchical functions. Higher order functions do not replace lower orders, but are superimposed on to them. To illustrate this principle a 1D case, thus for one edge in one direction, the refinement is shown in Fig. 5.

By adding extra shape functions, higher orders elements receive more DOF. The relationship between order and number of DOF n is as follows;

$$n(p) = \begin{cases} n = 8 \cdot p & \text{if } p < 4 \\ n = p^2 + 3 \cdot p + 6 & \text{if } p > 3 \end{cases}$$

The alternative is h-refinement where the elements do not get extra DOF, but the mesh is refined with smaller elements. This refinement is not used for several reasons. Firstly the elements need a certain size to correlate. Second the mesh should be regenerated and matrices K should be recalculated. Finally, as it is implemented in other global procedures, refinement is based on user experience. These disadvantages are not present for p-refinement as shown in the previous paragraph.

It is important to note that in our proposed method no uniform updating is done. And thus not simply fixed higher order elements are used. Only the regions where the elements are not able to describe the real displacement, and thus where the *error* is high, will be refined. The refinement (adding orders) is established as follows. The element to be

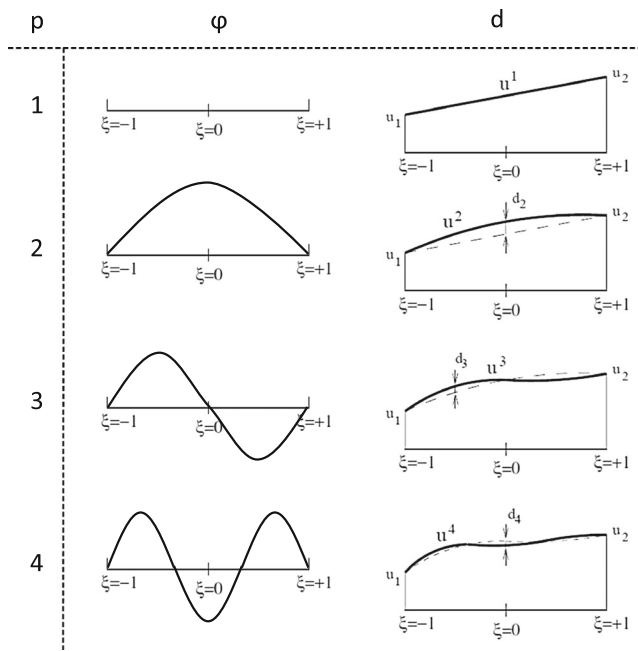


Fig. 5 1D representation of the principle of hierarchical shape functions

refined contains n DOF's, resulting in displacement field \mathbf{d} .

$$\mathbf{d} = \sum_{n,a} \Phi_n \delta_n \mathbf{e}_a \quad (30)$$

with

$$[K^n][\delta^n] = [F^n] \quad (31)$$

as element equations. When refining the element to \mathbf{d}' by adding m DOF's (e.g. updating from $p=3$ to $p=4$ then $m=5$) the displacement field, with $n' = n + m$ DOF's, becomes:

$$\mathbf{d}' = \sum_{n',a} \Phi_{n'} \delta_{n'} \mathbf{e}_a \quad (32)$$

Because the shape functions are independent, one obtains

$$\mathbf{d}' = \sum_{n,a} \Phi_n \delta_n \mathbf{e}_a + \sum_{m,a} \Phi_m \delta_m \mathbf{e}_a \quad (33)$$

Using the equation above in combination with equation (3), it can easily be shown that:

$$[K^{n'}][\delta^{n'}] = [F^{n'}] \quad (34)$$

where

$$[K^{n'}] = \begin{bmatrix} K^n & K^{nm} \\ K^{nm} & K^m \end{bmatrix} \text{ and } [F^{n'}] = \begin{bmatrix} F^n \\ F^m \end{bmatrix} \quad (35)$$

The independence of calculated coefficients is straightforward as the matrix K^n regarding the original element is simply reused in the matrix $K^{n'}$ representing the refined element. This makes refining the element in the global method more efficient. Each time an element is refined with extra DOF's, only the coefficients connected to the newly added

freedoms are calculated. The remaining coefficients can be copied.

Error Estimation

In adaptive finite element analysis, error estimation is a widely discussed topic [24, 25]. Lots of research has been done, and multiple approaches are developed. It is now the goal to transfer these estimators to the global method for DIC. In general, two main areas exist in error estimation: a-priori and a-posteriori estimators. In this proposal only a-posteriori error estimation is used [29], because no a-priori information about the experiment is known.

Basically, a-posteriori estimators exist in two groups. Namely recovery or residual based estimators. Recovery based error estimation was proposed by Zienkiewicz et al. [30, 31]. The principle is to extract/recover a 'more accurate solution' based on the current solution. The most popular example is the ZZ-estimator [30], where the recovered solution is found by using so-called 'super converged points'. These methods are sometimes called Single Pass Algorithms (SPA) as only one refinement pass is used. After the first calculation, the error is determined using a super convergent solution. Based on this error, the order needed for each element is determined. The calculation is performed again with the updated mesh, resulting in the final results. An other approach is using multiple passes (MPA), where after each calculation an error estimation is done and the mesh is refined [32]. In MPA residual based errors, pioneered by Babuska, can be used where the error is determined by calculating the residual of the finite element solution in each local space. The error estimator implemented is an MPA, as after each correlation the error will be checked and if necessary elements raised in order. The (local) error in measurand u is defined as:

$$e = u - \hat{u}, \quad (36)$$

where e is the local error, u is the exact solution and \hat{u} is the correlated, discretised solution. Measurand u can be displacement, strain or any other quantity of interest. From this local (point wise) error an element error can be determined. In FEA the norm used to describe the element error is the energy norm

$$\|e\| = \sqrt{\int_{\Omega} e^T L e \cdot d\Omega} \quad (37)$$

With L the self-adjointed operator. By the lack of material parameters not the energy norm but RMS norm is used. This is valid as scalar norms are similar to the energy norm [19].

$$\|e\| = \sqrt{\frac{\int_{\Omega} e^T e d\Omega}{\int_{\Omega} d\Omega}} \quad (38)$$



If this element error is used as an absolute error, the element should be update if:

$$\|e\| > \|\bar{e}\| \tag{39}$$

with $\|\bar{e}\|$ the permissible RMS error. Another approach is evaluating the element by relative error. Then indicator η is introduced:

$$\eta = \frac{\|e\|}{\|\hat{u}\|} \tag{40}$$

where

$$\|\hat{u}\| = \sqrt{\frac{\int_{\Omega} \hat{u}^T \hat{u} d\Omega}{\int_{\Omega} d\Omega}} \tag{41}$$

Leading to the updating condition:

$$\eta > \bar{\eta} \tag{42}$$

In this way, if the element error is known, elements to be refined are identified. In the following, calculation of the local error is presented. Starting from the definition of error:

$$e = u - \hat{u} \tag{43}$$

Based on Zienkiewicz’ work [31] the error is approximated by the use of a higher order. Here the higher order solution, one order higher than the current order p , is an approximation for the the exact solution:

$$e \cong \hat{u}^{p+1} - \hat{u}^p \tag{44}$$

The approximation is valid if it is assumed that the error goes down if the order goes up. Since calculating a higher order solution makes our current (lower order) solution useless, the previous solution is preferred instead of the next:

$$e < e' = \hat{u}^p - \hat{u}^{p-1} \tag{45}$$

Using this approximation, the error will always be overestimated, which is acceptable as it will yield a more accurate result. This principle, proposed by Zienkiewicz, is common as estimator in p-FE code [33]. To make the estimator independent of the history of the correlation, the error e' can be approximated as [25]:

$$e' \cong \sum_h \Phi_h \delta_h \tag{46}$$

with h denoting the highest orders of the element. Referring to the displacement function equation (4) based on shape functions (Fig. 4), the h denotes the functions in the last row as seen in Fig. 6.

If h is defined, e' equation (46) can be calculated resulting in element error $\|e\|$ equation (38).

$$\|e\| = \sqrt{\frac{\int_{\Omega} e'^T e' d\Omega}{\int_{\Omega} d\Omega}} \tag{47}$$

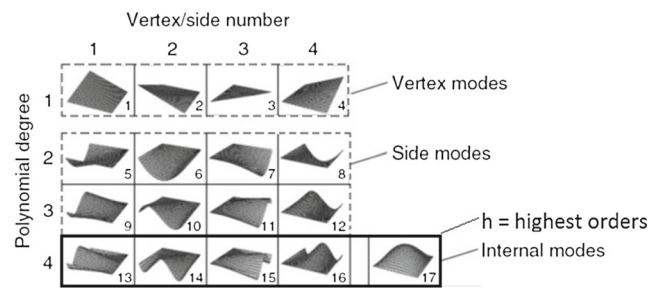


Fig. 6 Indication of shape functions h used for error estimation

and if

$$\|e\| > \|\bar{e}\| \tag{48}$$

then the element is updated. Note that the same reasoning is used for the relative error η . Because only parameters from the current solution are used, the calculation of the error is very efficient. This estimator can be classified as a MPA method, as at each stage the local error is estimated.

Flowchart p-DIC

To summarise all stated before, a simple flowchart of our new proposed method is shown in Fig. 7.

Performance

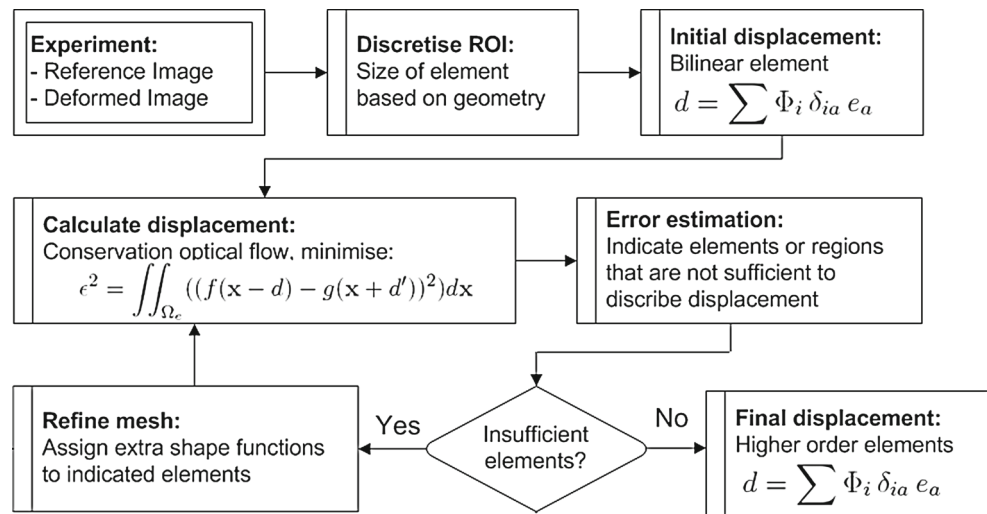
In previous sections the mathematical framework for the new algorithm was presented. The present section aims at a validation of the proposed algorithm, using measurements and spatial resolution. By way of comparison, the following definitions are firstly presented [34]

- **Measurand:** Object of measurement. Quantity of interest and submitted to the measurement process. In the present application mostly displacement or strain.
- **Resolution:** change in quantity being measured that causes a change in the corresponding indication greater than one standard deviation of the measurement noise. Resolution is comparable to precision.
- **Spatial resolution:** A measure indicating the distance between two independent data points. Spatial resolution is comparable to the detail of the method.

An in-depth comparison of different subset-based platforms has been performed by Bornet et al. [14]. Bornet et al. used sinusoidal deformation fields to assess the metrological performances of image correlation algorithms. Series of sinusoidal deformed images where generated with various frequencies and amplitudes. Results showed that general trends are strongly correlated with the underlying algorithms. A similar approach is used in this comparison, but



Fig. 7 Flowchart of the proposed p-DIC method



extensions are done to be applicable for both the local and global method. Comparable images and representations are used. The resolutions and the spatial resolution are plotted in one graph, as the combination of these two quantities indicate the performance of the methods. As can be predicted, both values are inversely related. Achieving a lower spatial resolution leads to an increase of the measurand resolution. For comparison, the in-house developed subset-based platform “MatchID 2D” is used [5]. In the p-DIC method the same libraries for interpolation and mathematical operations are used, leading to a more profound comparison. The influence of filters, interpolation and matrix calculation are ruled out in this way.

Methodology

Parameters

To perform an assessment of DIC, series of synthetic images are used. As reference image, an image of a real speckle pattern (Fig. 8) is used. The dimensions of the images are 1200 by 250 pixels².

As deformed images, numerically deformed images are used. These images are generated by altering the gray level distribution $f(\mathbf{x})$, representing the reference image. If the displacement field is defined by $\Phi_D(\mathbf{x})$, the deformed gray level distribution $g(\mathbf{x})$ is found by following relation:

$$g(\mathbf{x} + \Phi_D(\mathbf{x})) = f(\mathbf{x}) \tag{49}$$

The generation of the deformed images is done by using the finite element simulation of the experiment intended to be numerically reproduced [13]. The element size of that mesh is taken small enough to minimise the error. By imposing a

known deformation field, the error of the correlation can be assessed in different ways. First a local error is defined.

$$\Delta u(x, y) = u_{imposed}(x, y) - u_{measured}(x, y) \tag{50}$$

with $(x, y) \in ROI$. Globally, the root mean square error is defined by

$$RMS_g = \sqrt{\frac{1}{n} \sum_{x,y} [\Delta u(x, y)]^2} \tag{51}$$

The standard distribution and arithmetic mean are defined as:

$$\sigma_g = \sqrt{\frac{n \sum_{x,y} [\Delta u(x, y)]^2 - [\sum_{x,y} \Delta u(x, y)]^2}{n(n-1)}} \tag{52}$$

$$\overline{\Delta u}_g = \frac{\sum_{x,y} [\Delta u(x, y)]}{n} \tag{53}$$

Finally, some directional parameters are introduced. Directional is defined as using only data in the specified direction. The y-directional standard distribution and arithmetic mean are:

$$\sigma_y(x) = \sqrt{\frac{n \sum_y [\Delta u(x, y)]^2 - [\sum_y \Delta u(x, y)]^2}{n(n-1)}} \tag{54}$$

$$\overline{\Delta u}_{y(x)} = \frac{\sum_y [\Delta u(x, y)]}{n} \tag{55}$$

The x-directional parameters are analogously defined.

Measurand resolution

The resolution is determined by using a so-called self correlation test. Such a test implies the correlation between two images where no deformation is performed. Due to noise and other influences, a deformation field between both images is measured. For that reason the images used are the original pattern (Fig. 8) and the same image with an



added (numerical) Gaussian noise with a standard deviation of 1 %, general obtained for standard 8-bit cameras. The measurand resolution is defined as the global standard deviation σ_g of the biased measurand field [35].

Measurand spatial resolution

Traditionally, the spatial resolution is defined as the distance between two independent data points [35, 36]. For the local method, the closest distance between two independent data points is the subset size itself. In this case, two neighbouring subsets separated with the subset size from each other will use different pixels and thus remain completely independent. If subsets are closer to each other, they naturally overlap and use common pixels. As such they lose their independence and thus in the subset method the spatial resolution is the subset size. The step size only indicates the density in data points. This traditional definition is not applicable to global DIC as the area needed to correlate a data point is not clearly defined. Bornet et al. [14] assessed the metrological performances of different local image correlation algorithms using the sinusoidal deformation fields. As they assess different errors, no clear definition is provided for the spatial resolution. For that reason an alternative indication is used based on the fundamental work of Bornet et al. The spatial resolution will be evaluated as the lowest period (i.e. highest frequency) of a sinusoidal deformation that the method is able to reproduce before losing a certain percentage of amplitude. In this way, a poor resolution is a high value and an optimum value is a low one, similar as for the resolution. Thus as deformed image a unidirectional in-plane sinusoidal deformation field is introduced to the original speckle pattern. For displacement this equals:

$$\Phi_D(\mathbf{x}) = \begin{cases} d_x = a \cdot \sin(\frac{2\pi}{P} \cdot x) \\ d_y = 0 \end{cases}$$

where a is the amplitude and P the constant period. From this unidirectional in-plane sinusoidal deformation field, a 1D-displacement function R can be extracted using the directional average discussed before.

$$R(x) = \overline{\Delta u_y(x)} = \frac{\sum_y [\Delta u(x, y)]}{n} \tag{56}$$

The function R represents the average sine function the methods (local or global) are capable of reproducing. From

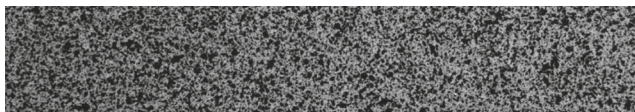


Fig. 8 Speckle pattern used for validation $1200 \times 250p^2$

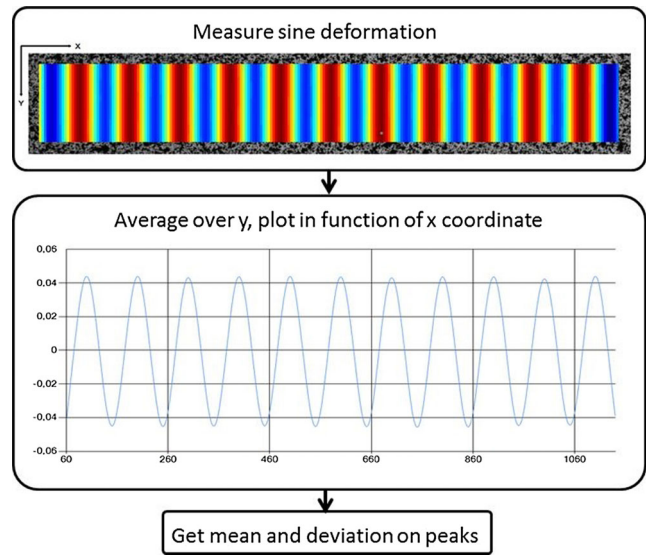


Fig. 9 Procedure for determining spatial resolution

the function R the absolute peaks are extracted, denoted as matrix $[A]$, as they represent the reconstructed amplitude. From these peaks average and deviation can be calculated.

$$\sigma_a = \sqrt{\frac{n \sum_p [A]_p^2 - [\sum_p [A]_p]^2}{n(n-1)}} \tag{57}$$

$$\mu_a = \frac{\sum_p [A]_p}{n} \tag{58}$$

The principle is shown in Fig. 9. The loss of amplitude is then defined as:

$$\Delta A = \frac{|a - \mu_a| + 3 \cdot \sigma_a}{a} \cdot 100 \tag{59}$$

By the use of $3 \cdot \sigma_a$ a certainty of 99.8 % on amplitude determination is obtained. As we defined the spatial resolution as the lowest period the method is able to reproduce with a amplitude loss of α , one has

$$Resolution = P \longleftrightarrow \Delta A = \alpha \tag{60}$$

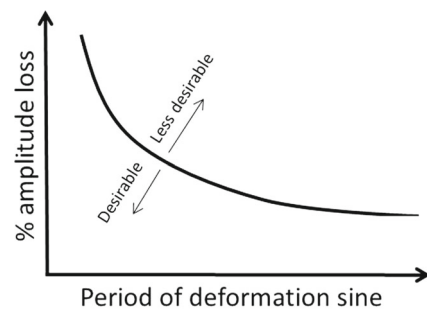


Fig. 10 Relation amplitude loss vs period of deformation



Table 1 Deformation parameters for the validation of displacements spatial resolution

Parameter	Value
a	5 pixels
P	50 $\xrightarrow{25}$ 200

where α is the percentage of allowed amplitude loss, which will be the criterion for the spatial resolution determination.

By applying this procedure for different frequencies, methods and settings, the loss of amplitude is known in function of frequency for each setting and method. The graphs resulting from this method are similar as in Fig. 10.

In this way the spatial resolution is mathematical determined using only the final deformation field, making it possible to determine the spatial resolution regardless of the method chosen. For this comparison error estimation and adaptive meshing is deactivated. This ensures that different settings are maintained to produce a graph similar as in Fig. 10. If these features were used, the algorithm would update the mesh (higher order) and no loss in amplitude can be measured.

Displacements Resolution and Spatial Resolution

In the following, the resolution and spatial resolution of the displacement is determined for the subset method, the Q8-DIC and p-DIC algorithm. The reference image is the original speckle pattern, the deformed images are the original pattern with an imposed Gaussian noise and unidirectional sinusoidal displacement field. For the resolution a Gaussian noise with a distribution of 1 % (2 gray values) is imposed. The in-plane unidirectional sinusoidal displacement field for the spatial resolution has the characteristics shown in Table 1.

MatchID is used to represent the subset-based approach. The algorithms receive settings shown in Table 2.

The resolution is clearly defined as the standard deviation of the measured artificial displacement field (see section “Measurand resolution”) while measuring the image with noise. The spatial resolution is defined in section “Measurand spatial resolution”. For each combination of method and setting (defined in Table 1) the period for a loss of amplitude ranging from 1 to 5 % can be determined

Table 2 Summarised correlation parameters used in the validation

	Subset method	p-DIC	Q8-DIC
Criterion	NSSD	NSSD	NSSD
Element size (pxl)	21 $\xrightarrow{10}$ 61	100 × 100	200 → 20
Element order	Quad	4 $\xrightarrow{1}$ 9	2

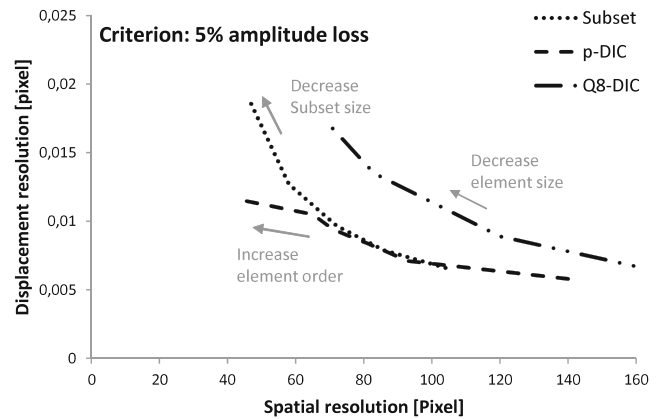


Fig. 11 Displacement vs spatial resolution for p-DIC, subset method and Q8-DIC. For the local (Q8-DIC) methodology, a decrease in subset dimensions (element size) is adopted horizontally from right to left. The introduced p-DIC, on the other hand, increases the element order from right to left. Spatial resolution criterion $\alpha = 5$

and coupled with the displacement resolution for that setup. The resulting graphs are shown in Figs. 11 ($\alpha = 5\%$) and 12 ($\alpha = 1\%$).

Figures 11 and 12 confirms some intuitive expectations. First of all, as expected, the spatial resolution decreases (more heterogeneous deformation) if smaller subsets or higher order elements are taken. Related to the gain in spatial resolution, a increase in resolution is observed. The increase is explained by the rising influence of noise in smaller or higher order elements. Previous research [16] proved that a global approach has less influence of noise for the same element/subset size. Here it’s further proved that for the same spatial resolution, the global method has a lower displacement resolution than the subset method. This can be expected as the global method obtains C^0 -continuity and thus obtains a smooth displacement field.

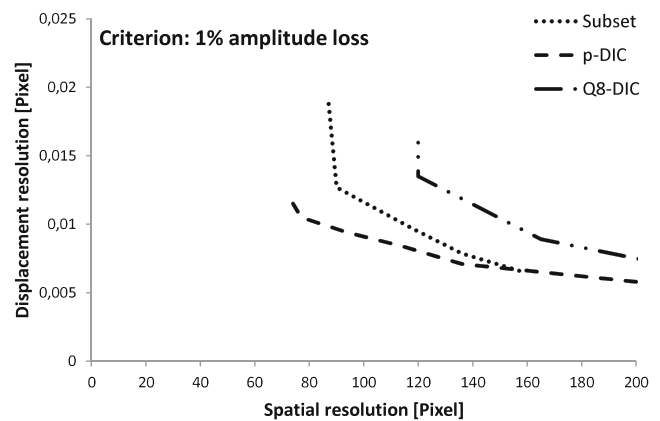


Fig. 12 Displacement vs spatial resolution for p-DIC, subset method and Q8-DIC. For the local (Q8-DIC) methodology, a decrease in subset dimensions (element size) is adopted horizontally from right to left. The introduced p-DIC, on the other hand, increases the element order from right to left. Spatial resolution criterion $\alpha = 1$



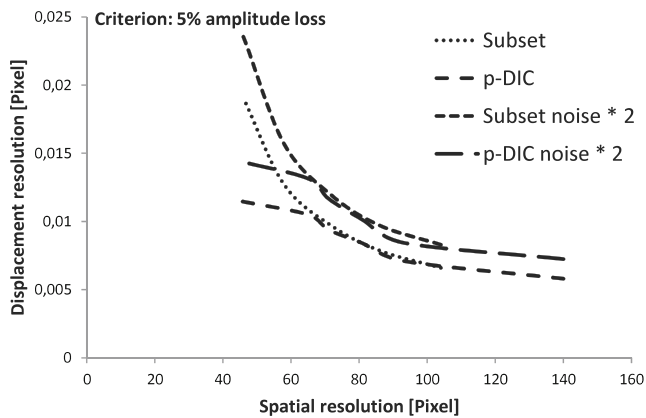


Fig. 13 Influence of noise on Displacement vs spatial resolution for p-DIC and subset method. Spatial resolution criterion $\alpha = 5$

Introducing higher orders in the global method keeps this low influence of noise but also lowers the spatial resolution, as more complex deformations can be represented. The graph also indicates that lowering the criterion α , increases the difference between the subset and p-DIC method. At 1 % the difference is larger than at 5 %. In general it can be concluded that for low heterogeneous applications (high spatial resolution - right side of Figs. 11 and 12) the subset, Q8-DIC and p-DIC are competitive. All have similar displacement resolutions for the same spatial resolution. For higher heterogeneous applications (low spatial resolution - left side of Figs. 11 and 12), the p-DIC has less displacement resolution than the local and Q8-DIC method. For example: at a spatial resolution of 50 and criterion of 5 %, the subset method has a resolution of 0.0165, as the p-DIC has a resolution of 0.011. Influence of the amount of the noise has been investigated, concluding that noise shifts both Figs. 11 and 12 equally up as illustrated in Fig. 13. Here the noise level is doubled (from 1 % to 2 %). The general conclusion is still valid with higher noise values. The data discussed clearly indicate that for high accurate (low α) low spatial resolutions (low P), the p-DIC method is more favourable than the subset or Q8-DIC method.

Strain Resolution and Spatial Resolution

The same procedures are followed for the strain resolution and the spatial resolution. The only difference is that not a sinusoidal displacement field but strain field is imposed and

Table 3 Deformation parameters for the validation of strains spatial resolution

Parameter	Value
a	0.05
P	40 \rightarrow 200

Table 4 Summarised correlation parameters used in the validation

	Subset method	p-DIC
Criterion	NSSD	NSSD
Element size (pxl)	21 \rightarrow 61	100 \times 100
Element order	Quad	4 \rightarrow 9
Step (pxl)	2	pixel
Strain window size	11 \rightarrow 51	n/a
Strain order	Q8	n/a

that only the subset and p-DIC method are investigated. The in-plane unidirectional sinusoidal strain field for the spatial resolution has the characteristics shown in Table 3. For the resolution, again a Gaussian noise with distribution of 1 % (2 gray values) is imposed.

The configurations for the algorithms are given in Table 4.

The resolution is still clearly defined as the standard deviation of the measured artificial strain field (see section “Measurand resolution”). The spatial resolution is defined in section “Measurand spatial resolution”. For each combination of method and setting (defined in Table 4) the period for a loss in amplitude ranging from 5 to 15 % can be determined and coupled with the strain resolution for that set-up. The resulting graphs are shown in Figs. 14 and 15.

The representation of the data will be the same as the plot used for the displacement. Here criteria 5 and 15 % are used. Note that the graphs for other subsets between 21 and 61 lay between both lines and are left out for obtaining clear graphs.

The data clearly indicates that again lowering the criterion for amplitude loss (determining the accuracy) increases the difference between the methods. The local method was not able to reproduce the strain fields with an accuracy

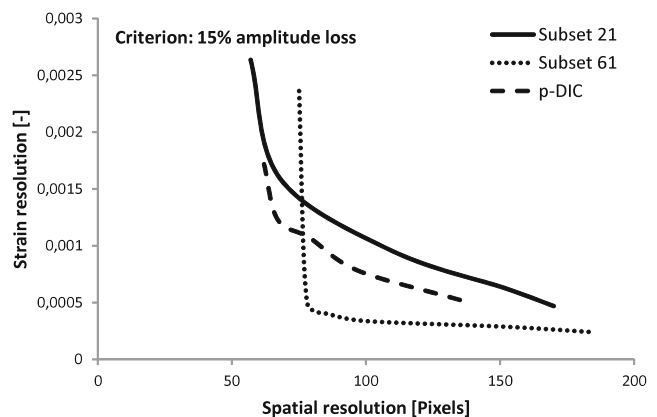


Fig. 14 Strain vs. spatial resolution for p-DIC and subset method. Spatial resolution criterion criterion 15 %

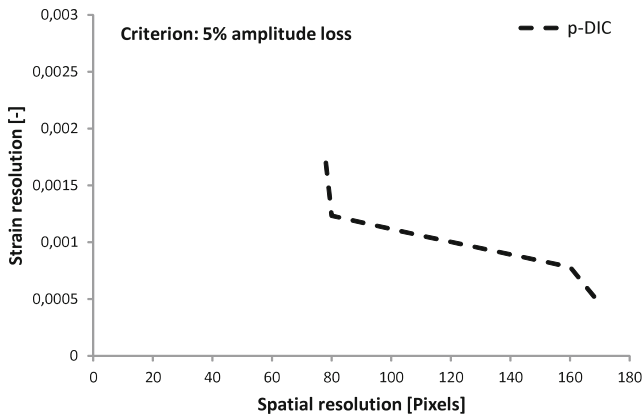


Fig. 15 Strain vs. spatial resolution for p-DIC and subset method. Spatial resolution criterion 5 %

of 5 %. Increasing this criterion made comparison possible showing that local and global become competitive. It is also noted that again the strain resolution is lower for the same spatial resolution, with increasing difference if the α is lowered. The same conclusion can be drawn as seen in the displacement resolutions, saying that for high accurate (low α) low spatial resolutions (low P) the p-DIC method clearly outperforms the local method.

Full Automatic Correlation

The p-DIC method, presented in chapter 2, is developed for measuring strains with minimal user dependency in applications producing a high gradient strain field. The validation of the p-DIC method is performed in chapter 3, showing that the p-DIC method is appropriate to be used in these low spatial resolution applications. To minimise user dependency on the results, an error estimator was introduced to adapt the mesh where necessary. Remind that the validation

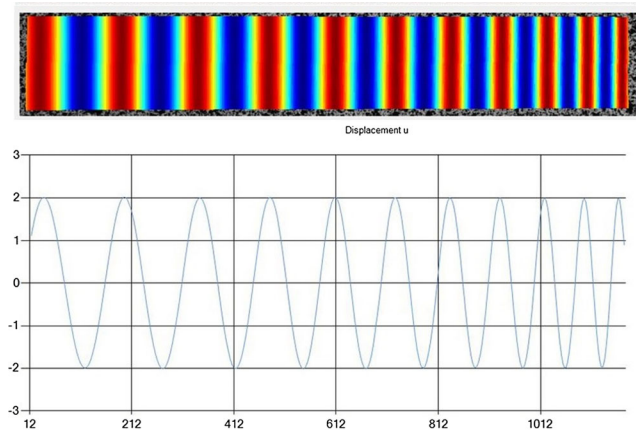


Fig. 16 Imposed unidirectional sinusoidal displacement field with varying frequency

Table 5 Correlation parameters for p-DIC

Parameter	Value
Interpolation	Bicubic
Correlation	NSSD
p-refinement	enabled
Uniform updating	4 th order
$\ e\ $	0.05

is performed without the error estimator to not alter the spatial resolution of the method. In this chapter the estimator is activated to prove the concept of the estimator.

The aim is to point out the independence of results obtained by p-DIC. The most important task of the estimator is to identify regions where the mesh is insufficient. Insufficient in this context means needing higher orders to describe the real displacement and thus needing a lower spatial resolution. To test this performance, again a unidirectional sinusoidal numerical deformed image is used. In contrast with previous methodology, a variation in spatial resolution is imposed.

$$\Phi_D(\mathbf{x}) = \begin{cases} d_x = a \cdot \sin[\frac{2\cdot\pi}{P_0} \cdot x + (\frac{2\cdot\pi}{P_1} - \frac{2\cdot\pi}{P_0}) \cdot \frac{x^2}{2L}] \\ d_y = 0 \end{cases}$$

Where P_0 is the begin period, P_1 the end period and L the length of the image. In this case $P_0 = 160$ pixels, $P_1 = 70$ pixels and $L = 1200$ pixels. The resulting field is shown in Fig. 16.

With this variation in spatial resolution, a similar variation should be found in the order distribution of the elements. Choosing larger or smaller elements will lead to respectively higher or lower orders. The input for the p-DIC algorithm is shown in Table 5.

These settings have the following proceeding. First, the mesh is uniformly updated until 4th order to prevent severe underestimation of the real displacement. Once the mesh reaches 4th order, the estimator is responsible for updating

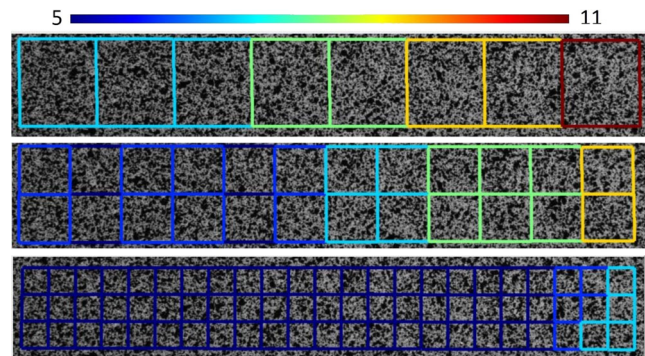


Fig. 17 Distribution of element orders for the correlation of a displacement field with varying needed spatial resolution for elements ranging from 50x50 to 150 × 150 pixels

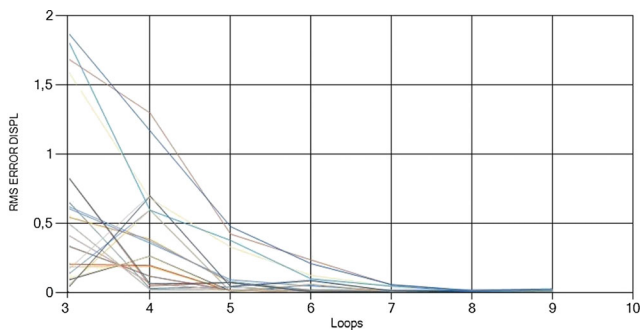


Fig. 18 Trend error estimation value for correlation with element size 100×100

the mesh. If the element error indicator $\|e\|$ equation (47) is larger than $5 \cdot 10^{-2}$ pixels, that element is refined. Running p-DIC with these settings and using element sizes ranging from 50×50 to 150×150 (= user dependent input), the algorithm yields order distributions as shown in Fig. 17.

Based on the indicator equation (47), the error plot for element size 100 (middle mesh in Fig. 17) is shown in Fig. 18. The x-axis represents the refinement loop. The y-axis represents the error indicator value. As seen in the settings, uniform updating is done for four loops, after that the adaptive procedure takes over. Each line on the graph represents an element's indicator in all the loops. The converging behaviour is clearly seen and in loop 9 all elements are converged.

The convergence graphs for the other mesh sizes are similar. The convergence and order distribution proves that the estimator is able to refine the mesh properly, as needed by spatial resolution. The left side of Fig. 17, where the deformation is less heterogeneous, has lower orders than the right side. Also, the large elements are higher order than the small elements. This experiment shows that the measurement is now less dependent from user input. The algorithm will automatically converge to the proper order to represent the real displacement field, and thus having an user independent spatial resolution. This is in contrast to the subset method where the spatial resolution is linked to the subset size, chosen by the user. No feedback is given on loss of spatial resolution, in contrast to the p-DIC. In Table 6 errors of the correlation for the three mesh sizes are presented. The accuracy is RMS_g equation (51) based on the known theoretical

Table 6 Accuracy, resolution and spatial resolution for p-DIC using different element sizes

Size	Accuracy	Resolution	Spatial resolution
50 x 50	1.88 %	0.72 %	1.22 %
100 x 100	1.85 %	0.50 %	1.15 %
150 x 150	2.25 %	0.37 %	2.00 %

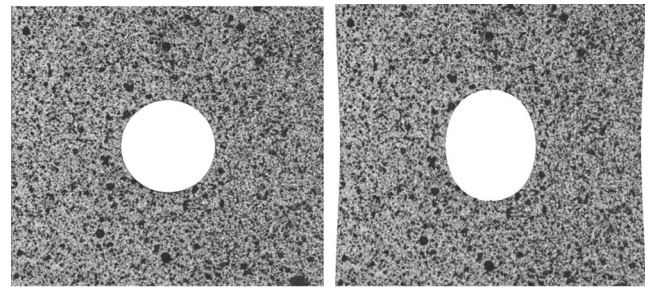


Fig. 19 Numerically simulated tensile test with imposed noise. On the left the reference image, on the right the deformed image

imposed displacement field. The resolution is the standard deviation of the measured displacement field obtained by correlating a noised reference image (see section “Measurand resolution”). The spatial resolution is the percentage of amplitude loss in the reconstruction of a sinusoidal displacement field (see section “Measurand spatial resolution”).

The results, shown in Table 6, indicate a clear conclusion. Starting with a bigger mesh influences the spatial resolution slightly. The spatial resolution only rises 0.78 % for an element area increase of 900 %. The estimator will update the mesh till convergence, and thus till the mesh is able to reproduce the real displacement. The resolution slightly increases when smaller elements are taken. As the accuracy is a combination of resolution and spatial resolution the same conclusion stands.

Using the p-DIC method, one thus chooses the biggest mesh possible. If the correlation does not converge, a smaller mesh should be chosen. If the method converges, one is sure that regardless of the mesh chosen the spatial resolution is low enough if the setting for the estimator is appropriate. By using the biggest mesh that has convergence, one results a solution with enough spatial resolution and the lowest resolution.

Application to a Tensile Test

For a more realistic situation, a tensile test is numerically simulated. In the image noise is introduced to be as realistic as possible. A holed aluminium specimen is used,

Table 7 Correlation parameters p-DIC

Criterion	NSSD	–
Interpolation	Bicubic	–
Shape function	Automatic update	–
Min order	4	–
Element size (pxl)	100×100	<i>pixel</i> ²
$\ e\ $	0.025	<i>pixel</i>

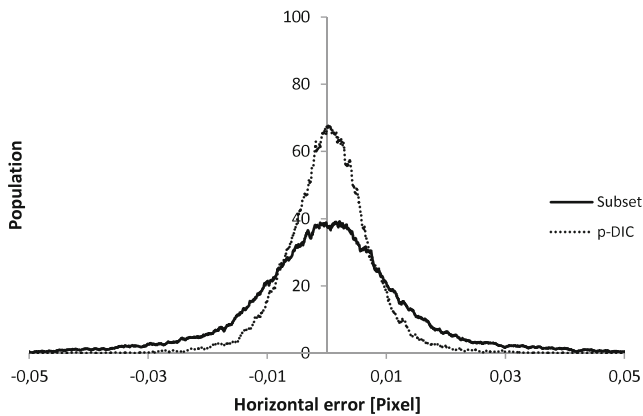


Fig. 20 Distribution absolute error horizontal displacement for tensile test on holed specimen using subset and p-DIC

producing a heterogeneous strain field. Extensive research has been done by Wang et al. [37] for selecting correct correlation parameters for the subset method. It is stated that the choice of parameters is critical for reaching the optimum between noise reduction and spatial resolution. For the experiment the same artificial images as in [37] will be used, so the same optimum parameters can be selected for the subset method. The used images are shown in the Fig. 19 where the left image represents the reference image and the right the deformed image.

As stated by Wang et al this experiment has an optimum subset size of 25 with affine shape function (based on speckle pattern, noise, strain state, criterion ...). The strain window should be bilinear with size 9. For p-DIC, the settings shown in Table 7 are used.

Notice that the choice of element size is not critical, uniform updating is performed until 4th order and the estimator will refine the mesh automatically. That indicates the data is less user dependent, as each correlation starts with the same settings (error estimator) and adapts it self during the correlation. Also, both methods use the same

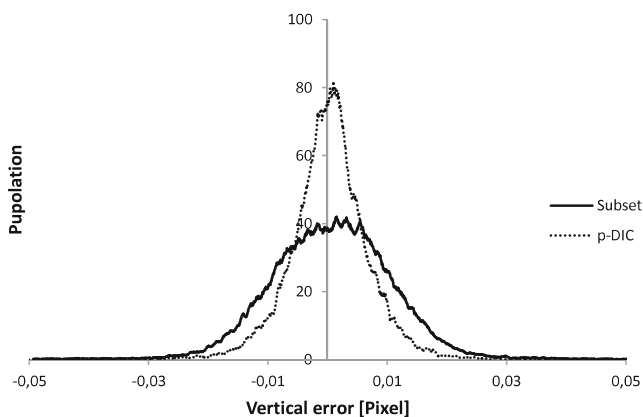


Fig. 21 Distribution of error in vertical displacement for tensile test on holed specimen using subset and p-DIC

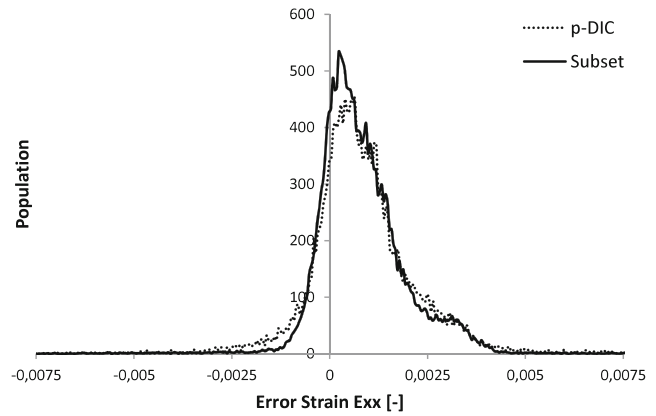


Fig. 22 Distribution of error in strain ϵ_{xx} for tensile test on holed specimen using subset and p-DIC

interpolation library to make the comparison more profound. As the images are numerically deformed, the theoretic displacement and strain field is known. Based on these fields, the distribution of the errors are shown in Fig. 20 till Fig. 23. The error is defined as the difference between imposed an measured deformation.

The first conclusion coming from Figs. 20 and 21 is that the distribution of the error in p-DIC displacements have less variance than the ones from the subset method, although for this method the optimal settings where used. Remark that these optimal settings for the subset method can only be found by the knowledge of the “true” deformation. Development of an experimental simulator is on its way so that different settings can be checked, yielding the optimal correlation parameters [38]. Currently obtaining these parameters is not possible yet and the settings has to be estimated by user experience. Even if the simulator was used, again user dependent input will be needed in the simulator (model, noise, material, ...) whereas the p-DIC refines only based on the experimental data without any model or pre-knowledge.

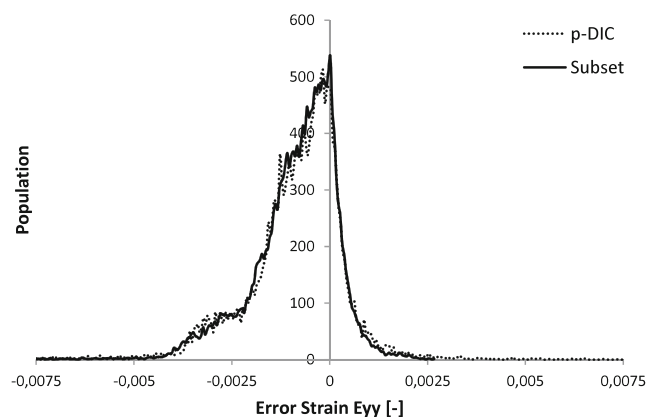


Fig. 23 Distribution of error in strain ϵ_{yy} for tensile test on holed specimen using subset and p-DIC

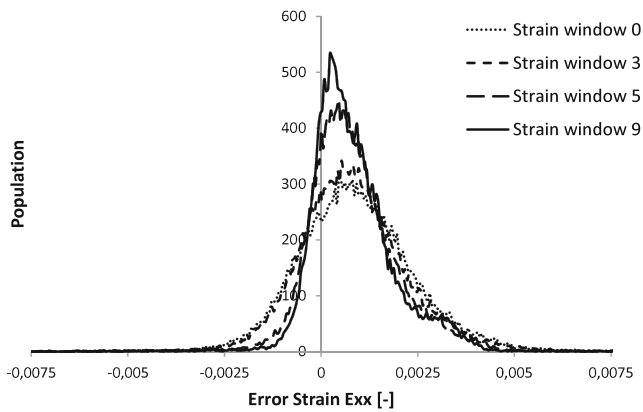


Fig. 24 Distribution of error in Exx using various strain window sizes for tensile test on holed specimen

Secondly, Figs. 22 and 23 show that the use of a strain window greatly improves the accuracy despite the noisy measurement. The results (variance) for displacement field are better (smaller) for the p-DIC method than the subset method. More accuracy is obtained in the strain field by smoothing the displacement field until calculated strains are acceptable. The accuracy is here obtained by applying the correct filter, dependent on the used step and strain window, and is thus very user dependent. This effect of change in data is shown in the Fig. 24.

The graph clearly shows the change in error, if the strain window is changed. Increasing the window reduces the noise effect, reducing the variance. Remark that if even larger strain windows were used, the error distribution starts widening again due to the lack of spatial resolution. For this reason, increasing the size of the window is limited by the spatial resolution, which is not known in a normal test. There thus exists a window of acceptable values which is not known, making it cumbersome to find these acceptable settings. Because the p-DIC obtains the derivatives directly, without any smoothing, this problem does not occur.

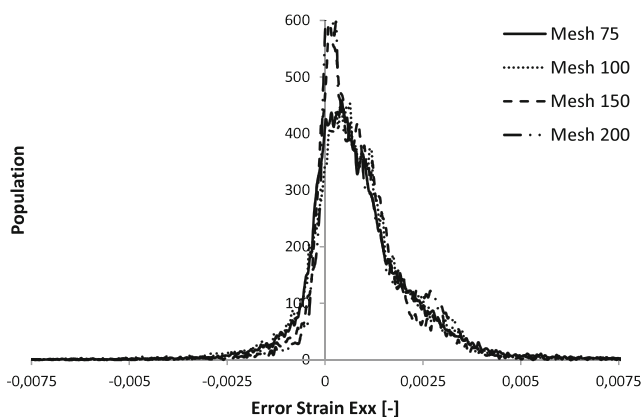


Fig. 25 Distribution of error in Exx with various element sizes for tensile test on holed specimen

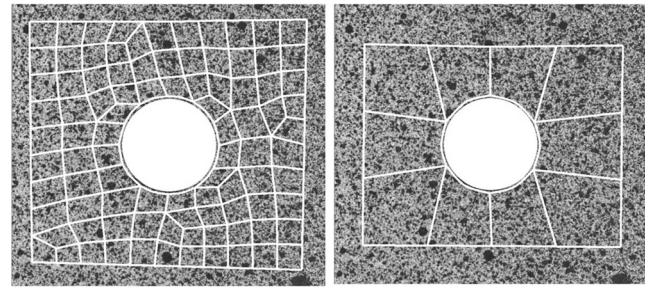


Fig. 26 Left: Mesh size 75×75 . Right: Mesh size 200×200 pixels

To prove the statements made earlier the same graph is produced for the p-DIC where the mesh ranges from 75×75 to 200×200 pixels resulting in Fig. 25 representing the change in error in function of the mesh choice. Other settings like $\|e\|$ and uniform updating order are not altered.

The graph confirms the conclusions made earlier: the p-DIC method is less dependent of user's input than the subset method. There is a small change in the error distribution for an extreme range of elements (increment of 166 %). The smallest and biggest elements are shown in Fig. 26. Although the use of small elements (size 75) is less favourable (see section “Full Automatic Correlation”), the method still yields acceptable results comparable to the optimal subset size. As stated before, larger elements are more favourable for the p-DIC method, as noise has less influence and thus large elements have to be used. Once the elements are large and reaching convergence the difference is minimal (size 125×125 till 200×200). The size is limited by the geometry of ROI or the lack of convergence indicated by the estimator. Still keep in mind that although for the p-DIC methods the least favourable settings where used, similar results are obtained as by the subset method (see Figs. 22 and 23).

Conclusion

In this paper a new global DIC algorithm is presented. The algorithm adopts features from the concept of adaptive FEA. The region of interest is described by an adaptive element mesh. A p-refinement scheme is implemented so that the elements in the mesh are capable of rising in degrees of freedom when the error estimators indicate them to do so. Using measurand resolution and spatial resolution, a validation of the traditional local and newly presented p-DIC is performed. Results from the validation indicate that the p-DIC method has a lower measurand resolution for the same spatial resolution compared to the local method. Also from the strain validation can be concluded that for the accurate measurement of low spatial strain fields the p-DIC method

is more favourable than the local method. Beside the advantage in performance at optimal settings, an other major advantage is that the method becomes less user dependent by using the self-adapting mesh. The spatial resolution is, in comparison to the local method, not limit by initial user settings. Future work is mainly aimed on the further development of the error estimators as they are key in the p-DIC procedure.

Appendix: Legendre Shape Functions

Legendre shape functions are a combination of function $P_p(\chi)$:

$$P_p(\chi) = \frac{1}{(p-2)!2^{p-2}} \frac{d^{p-2}}{d\chi^{p-2}} [(1-\chi^2)^{p-1}] \quad (61)$$

In a p-element shape functions are assigned to nodes, edges or faces identified in Fig. 27.

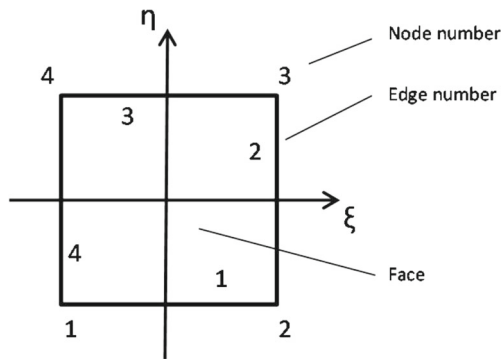


Fig. 27 Element nodes, edges and face

The shape functions that can be used are shown in Table 8 with p the polynomial order.

Table 8 Hierarchical shape functions

Object	Shape function
Node 1	$P_0(\xi)P_0(\eta)$
Node 2	$P_1(\xi)P_0(\eta)$
Node 3	$P_1(\xi)P_1(\eta)$
Node 4	$P_0(\xi)P_1(\eta)$
Edge 1	$P_p(\xi)P_0(\eta)$
Edge 2	$P_1(\xi)P_p(\eta)$
Edge 3	$P_p(\xi)P_1(\eta)$
Edge 4	$P_0(\xi)P_p(\eta)$
Face	$\sum_{k=1}^{p-3} P_{k+1}(\xi)P_{p-1-k}(\eta)$

References

- Avril S, Bonnet M, Bretelle A, Grediac M, Hild F, Ienny P, Latourte F, Lemosse D, Pagano S, Pagnacco E, Pierron F (2008) Overview of identification methods of mechanical parameters based on full-field measurements. *Exp Mech* 48:381–402
- Rastogi PK (2000) *Photomechanics: topics in applied physics*. Springer
- Sutton M, Orteu J, Schreier H (2009) *Image correlation for shape, motion and deformation measurements*. Springer
- Lagattu F, Brillaud J, Lafarie-Frenot MC (2004) High strain gradient measurements by using digital image correlation technique. *Mater Charact* 53:17–28
- MatchID MatchID 2D Software. <http://www.matchid.org>
- Dantec Dynamics Dantec DIC
- GOM optical measuring techniques Aramis 2D Software. <http://www.gom.com/EN/index.html>
- Correlated solutions Inc Vic-2D Software. <http://www.correlatedsolutions.com>
- LaVision Davis Software. <http://www.lavision.de/en/products/davis.php>
- Lava P, Cooreman S, Debruyne D (2010) Study of systematic errors in strain fields obtained via dic using heterogeneous deformation generated by plastic fea. *Opt Las Eng* 48:457–468
- Pan B, Asundi A, Xie H, Gao J (2009) Digital image correlation using iterative least squares and point wise least squares for displacement field and strain field measurements. *Opt Las Eng* 45:865–874
- Pan B, Qian K, Xie H, Asundi A (2008) Two-dimensional digital image correlation for in-plane displacement and strain measurement: a review. *Meas Sci Technol* 20:17
- Lava P, Cooreman S, Coppieters S, De Strycker M, Debruyne D (2009) Assessment of measuring errors in dic using deformation fields generated by plastic fea. *Opt Las Eng* 47:747–753
- Bornert M, Bremond F, Doumalin P, Dupre JC, Fazzini M, Grediac M, Hild F, Roux S, Mistou S, Molimard J, Orteu JJ, Robert L, Surrel P, Vacher Y, Wattrisse B (2009) Assessment of digital image correlation measurement errors: methodology and results. *Ex Mech* 49:353–370
- Cheng P, Sutton M. A, Schreier H. W, McNeill S. R (2002) Full-field speckle pattern image correlation with b-spline deformation function. *Ex Mech* 42:344–352
- Besnard G, Hild, Roux S (2006) “finite-element” displacement field analysis from digital images. *Ex Mech* 46:789–803
- Pan B (2010) Recent progress in digital image correlation. *Ex Mech* 51:1223–1235
- Tong W (2005) An evaluation of digital image correlation criteria for strain mapping applications. *Strain* 41:167–175
- Zienkiewicz OC, Taylor RL (2000) *The finite element method. Volume 1: the basis*
- Hild F, Roux S (2011) Comparison of local and global approaches to digital image correlation. *Ex Mech* 52:1503–1519
- Leclerc H, Perie J, Roux S, Hild F (2009) Integrated digital image correlation for the identification of mechanical properties. *Comput Vis/Comput Graph Collab Tech* 5496:161–171
- Hild F, Roux S, Gras R, Guerrero N, Marante M. E, Florez-Lopez J (2009) Displacement measurement technique for beam kinematics. *Opt Las Eng* 47:495–503
- Mortazavi F (2013) Development of a global digital image correlation approach for fast high-resolution displacement measurements. PhD thesis, ECOLE POLYTECHNIQUE DE MONTRÉAL
- Babuska I, Whiteman JR, Strouboulis T (2011) *Finite elements an introduction to the method and error estimation*. Oxford University Press

25. Akin JE (2005) Finite element analysis. With error estimators. Elsevier
26. Szabo B, Duster A, Rank E (2004) The p-version of the finite element method. Encyclopedia of Computational Mechanics
27. Chongy H (1990) An inverse transformation for quadrilateral isoparametric elements. *Finite Elem Anal Des* 7(2):159–166
28. Szabo B, Babuska I (1991) Finite element analysis. Wiley
29. Gratsch T, Bathe KJ (2003) A posteriori error estimation techniques in practical finite element analysis. *Comput Struct* 83:235–265
30. Zienkiewicz OC, Zhu JZ (1992) The superconvergent patch recovery and a posteriori error estimates. *Int J Numer Methods Eng* 33(7):1331–1364
31. Zienkiewicz OC, Zhu JZ, Gong NG (1989) Effective and practical h-p-version adaptive analysis procedures for the finite element method. *Int J Numer Methods Eng* 25(4):879–891
32. PTCUniversity (2012) The h- and p-versions of finite elements
33. Promwungkwa A (1998) Data structure and error estimation for an Adaptive p-Version. PhD thesis, State University Virginia
34. Chrysochoos A, Surret Y (2012) Chapter 1. Basics of metrology and introduction to techniques. Wiley
35. Grediac M, Sur F (2014) Effect of sensor noise on the resolution and spatial resolution of displacement and strain maps estimated with the grid method. *Strain* 50(1):1–27
36. (2007) ISO/IEC guide 99 - International vocabulary of metrology – Basic and general concepts and associated terms (VIM) ISO
37. Wang Y, Lava P, Coppieters S, De Strycker M, Van Houtte P, Debruyne D (2012) Investigation of the uncertainty of dic under heterogeneous strain states with numerical tests. *Strain* 48(6):453–62
38. Rossi M, Lava P, Pierron F, Debruyne D, Sasso M (2014) Error assessment on combining dic and vfm to design an optimized experimental set-up for material identification. Submitted - International Journal for Numerical Methods in Engineering